

NUMERIČNO MODELIRANJE VOZIŠČA OJAČENEGA Z GEOCELICAMI IN PRIMERJAVA Z LABORATORIJSKIMI EKSPERIMENTI

Samo Peter Medved (vodilni avtor)

Lineal d.o.o
Maribor, Slovenija
E-pošta: samo.medved@lineal.si

Bojan Žlender

Univerza v Mariboru,
Fakulteta za gradbeništvo, prometno inženirstvo in arhitekturo
Smetanova 17, SI-2000, Maribor, Slovenija
E-pošta: bojan.zlender@um.si

Stanislav Lenart

Zavod za gradbeništvo Slovenije (ZAG)
Ljubljana, Slovenija
E-pošta: stanislav.lenart@zag.si

Primož Jelušič

Univerza v Mariboru,
Fakulteta za gradbeništvo, prometno inženirstvo in arhitekturo
Smetanova 17, SI-2000, Maribor, Slovenija
E-pošta: primoz.jelusic@um.si

Izvleček

Članek opisuje, na kakšen način lahko izboljšamo uporabnost fleksibilnih voziščnih konstrukcij z uporabo geocelic. V ta namen smo z laboratorijskimi preizkusi preizkušali dva tipa voziščnih konstrukcij (z in brez ojačitve z geocelicami), ki smo jih obremenjevali z dinamično obtežbo, ki je simulirala prometno obremenitev. Preizkušance smo obremenjevali istočasno tako z vertikalno kot horizontalno obremenitvijo z namenom vzpostaviti kompleksno napetostno stanje (rotacija smeri glavnih napetosti). Predstavljena je primerjava med obnašanjem konvencionalne fleksibilne voziščne konstrukcije in voziščne konstrukcije ojačene z geocelicami. Izdelan je bil numerični model laboratorijskih preizkusov in predstavljena je primerjava z rezultati laboratorijskih obremenilnih preizkusov. Laboratorijski preizkusi so bili izvedeni z napravo TLS – simulatorjem prometnih obremenitev, medtem ko je bilo numerično modeliranje izvedeno z uporabo naprednih modelov po metodi končnih elementov (MKE), ki opisujejo trajne deformacije in napetostno stanje nevezanega nosilnega sloja iz kamnitega materiala. Razvoj trajnih deformacij voziščne konstrukcije brez in z ojačitvijo z geocelicami je prikazan na numeričnem modelu in preverjen z rezultati eksperimentov.

Ključne besede

fleksibilna vozišča, ojačitev, geocelice, simulator prometnih obremenitev, trajne deformacije, numerično modeliranje

MODELING OF A GEOCELL-REINFORCED PAVEMENT: AN EXPERIMENTAL VALIDATION

Samo Peter Medved (corresponding author)

Company Lineal d.o.o
Maribor, Slovenia
E-mail: samo.medved@lineal.si

Bojan Žlender

University of Maribor,
Faculty of civil engineering, transportation engineering and
architecture
Maribor, Slovenia
E-mail: bojan.zlender@um.si

Stanislav Lenart

Slovenian national building and civil engineering institute (ZAG)
Ljubljana, Slovenia
E-mail: stanislav.lenart@zag.si

Primož Jelušič

University of Maribor,
Faculty of civil engineering, transportation engineering and
architecture
Maribor, Slovenia
E-mail: primoz.jelusic@um.si

Keywords

flexible pavement, reinforcement, geocell, traffic load simulator, permanent deformation, numerical modeling

Abstract

This article details how the serviceability of a flexural pavement structure is improved by incorporating the Cellular Confinement System (geocells). For this purpose, two different pavement structures, with and without embedded geocells, were manufactured in a laboratory and an accelerated traffic type of loading was applied. The vertical and horizontal cyclic loads were applied simultaneously to simulate the effect of principal stress rotation. A comparative study between the conventional flexible pavement and the geocell-reinforced flexible pavement is presented. Additionally, numerical models of the laboratory tests were built and the results were compared. The simulation of the experimental tests using the Traffic Load Simulator (TLS) are carried out using the FEM and advanced models that describe the permanent strain behavior of the unbound granular material. The development of permanent deformation within the pavement structure, with and without the geocells, is also presented through the numerical model, which was verified by the experimental results.

1 INTRODUCTION

A pavement structure is a geometrically simple, multi-layered structure. The upper layers are formed by a bound material such as asphalt or concrete, while the lower-base and sub-base layers consist of unbound stone aggregate mixtures. The sub-grade layer under the pavement structure is an embankment or natural ground with features created by geological processes. Reinforcement can be introduced into the pavement structure to improve its cost-effectiveness and to extend the serviceable life of the structure.

Within the research presented in this article, geocell reinforcement is used to optimize the resources used to construct a solid, stabilized base and sub base for the pavement. The research goal was to prove the reduction of lateral as well as vertical movements of the soil particles in a pavement structure when a three-dimensional geocell confinement is used. [1].

Experimental and theoretical studies, which investigate the reinforcement mechanisms and failure modes of pavements reinforced with geocells, are described in the literature [2], [3]. Experimental studies carried out by Pokharel et al. [4] show that the installation of a geocell with a higher elastic modulus increases the stiffness and bearing capacity of a pavement. Accelerated pavement testing of unpaved roads with geocell-reinforced sand bases have been presented by Yang et al. [5]. Based on

the test results, they concluded that geocells significantly improve the stability of unpaved roads with sand bases and reduce the amount of permanent deformation. However, less experimental studies have been carried out on paved structures reinforced with geocells. An analysis and design methodology for the use of geocells in flexible pavements was proposed by Babu et al. [6]. Menegelt et al. [7] show the effect of the geocell on the resilient modulus dependent on the infill material. Resilient modulus tests were conducted on two coarse-grained soils (gravel and sand) and a fine-grained soil (lean silty clay) in a large-size cell with and without the geocell confinement. Singh et al. [8] presented a comparative study looking at a conventional flexible pavement and a geocell-reinforced flexible pavement. The results show a significant improvement in the bearing capacity when using geocell reinforcement.

This article presents the laboratory test results for a flexible pavement structure subjected to traffic loading, which was simulated by applying a synchronized vertical and horizontal cyclic load. A special testing device, named the Traffic Load Simulator (TLS), was constructed at the Slovenian National Building and Civil Engineering Institute (ZAG) for this purpose. In contrast to other similar experimental researches the TLS introduces vertical and horizontal cyclic loads to take into account the specifics of traffic loading, which results in vertical and horizontal normal stresses as well as non-zero values of the shear stress. The latter causes

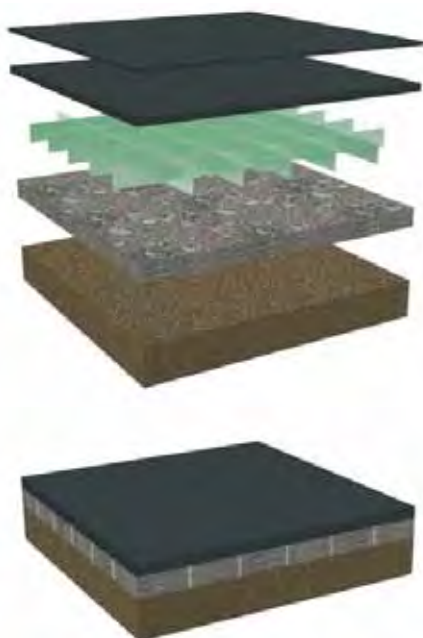


Figure 1. Scheme of a pavement structure reinforced with geocells.

the rotation of the principal stress axis. The impact of embedded geocells (Fig. 1) upon the rutting development, permanent deformation of the pavement structure and its vertical distribution in the base layer are presented. Additionally, this article presents a model for the rutting prediction based on a mechanistic-empirical method for flexible pavements using the layered elastic model. The developed model is compared to the experimental results of TLS tests to determine the accuracy of the proposed model.

2 EXPERIMENTAL PROGRAM

The arrangement of the laboratory test, the materials used and the details of the experimental program are described in this section. The laboratory test equipment with the Traffic Load Simulator (TLS) is presented in Fig. 3. Two specimens of paved road sections, 0.4 m long, 0.4 m wide and 0.51 m deep, were constructed for the purposes of the experiments in the laboratory. To enable particularities of the traffic load simulation with the principal stress axis rotation, specimens were constructed within 17 rigid aluminium frames. Free, non-frictional movements of the frames were allowed in the horizontal direction. The height of each aluminium frame is 3 cm and the internal layout dimensions are 40 cm × 40 cm. The loading in the vertical direction was applied with a full rubber tire attached to a hydraulic piston. The pavement structure was placed on the base of the loading frame and thereby rigidly supported in the vertical direction. The horizontal loading was applied through the lower aluminium frame with a horizontal hydraulic piston. The horizontal force is measured at the rigidly supported, upper aluminium frame.

Two accelerated pavement tests with multiple stage loading were performed on test specimens without geocells (TLS1) and with geocells directly under the asphalt layer (TLS3).

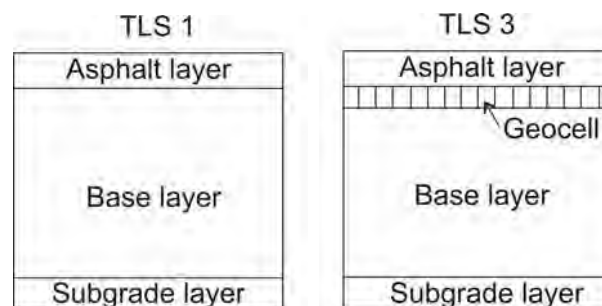


Figure 2. Test specimens without geocell and with geocell reinforcement.

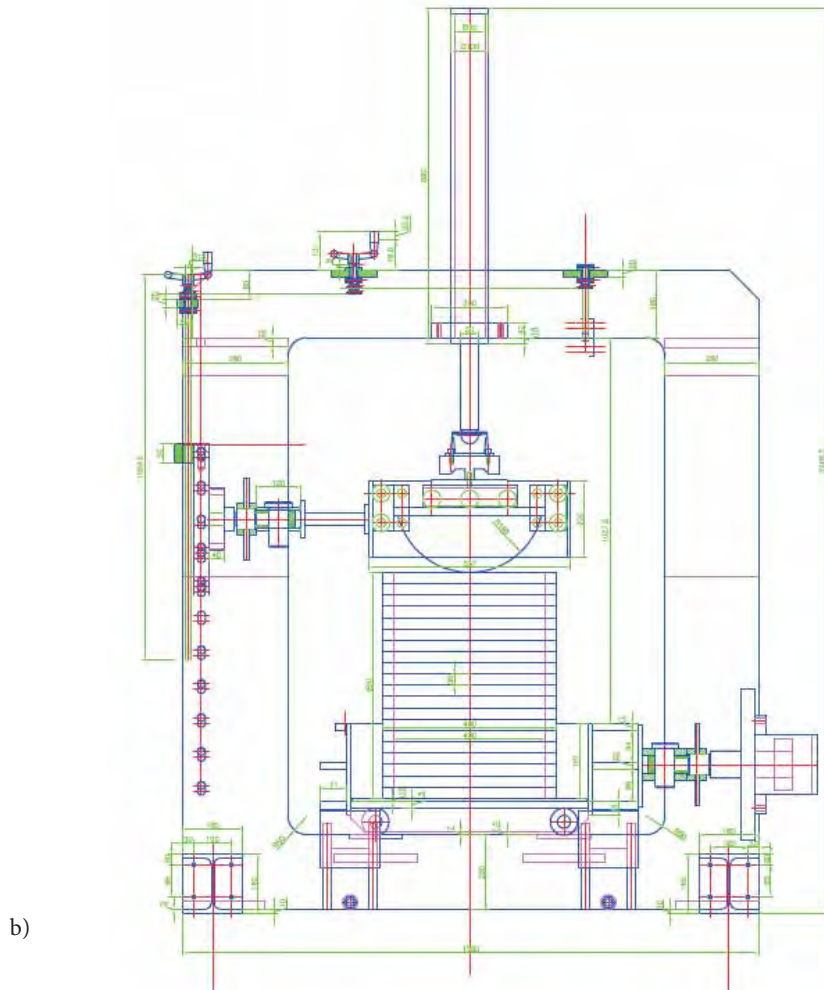
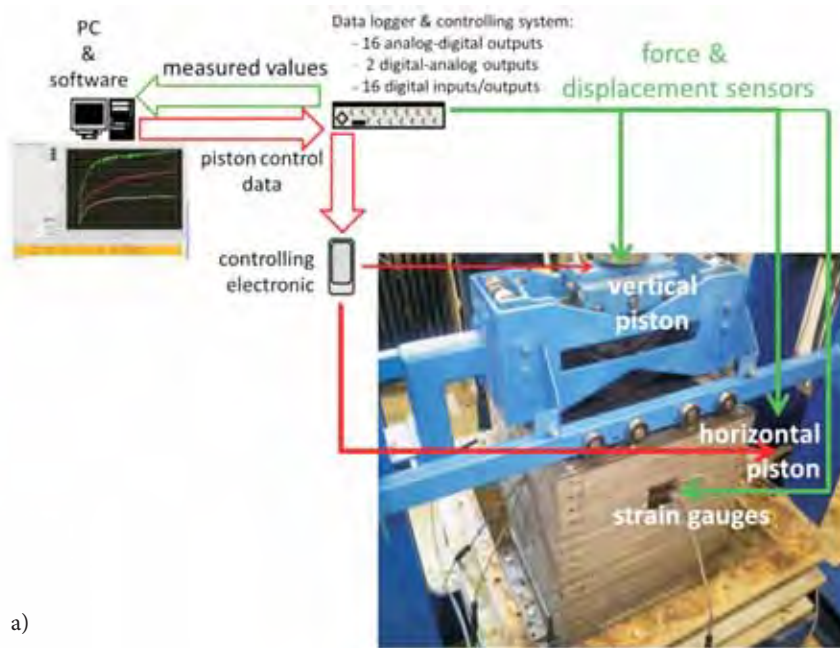


Figure 3. The laboratory test equipment: Traffic Load Simulator (a); Scheme of apparatus (b).

2.1 Material properties

2.1.1 Properties of asphalt

The impact of the type of asphalt used in relation to the deformation characteristics of the pavement was not researched in this study. Thus it was an aim to disable the asphalt effect by using the same type of asphalt layer in the case of the geocell-reinforced and unreinforced specimens. The asphalt mix, AC8 surf B50/70 A3, was prepared in a fixed asphalt mixing plant and left to cool. It was delivered to the laboratory in containers. When the test specimens were constructed in the laboratory, asphalt was heated up to approximately 150°C and manually compacted into 3-cm-thick surface layers. Details about the characteristics of the asphalt layer after the compaction are presented in Table 1. The main aim of preparing the asphalt layer was to minimize the possible differences between the asphalt layers of both test specimens.

Table 1. Characteristics of the material being compacted into test specimens.

		TLS 1	TLS 3
Asphalt	density, ρ (kg/m ³)	2401	2274
	density, ρ (kg/m ³)	2160	2090
Gravel	Water content, w (%)	5.51	5.70

2.1.2 Properties of Geocells

Geocells (Fig. 4) are recognized as a suitable geosynthetic reinforcement for granular soils to support static and moving wheel loads on roadways. The stiffness of the geocells has been identified as a key influencing factor for geocell reinforcement, and hence the rigidity of the entire pavement structure. Laboratory wheel load-



Figure 4. Geocells used in this study.

ing tests have shown that the performance of geocell-reinforced bases depends on the elastic modulus of the geocell. The Salvaverde type [9] of geocells has been used in this laboratory test. They are manufactured from a high-density polyethylene (HDPE) material. The height of the Geocells used was 5 cm, size (50 cm × 50 cm), the acceptable load stated by the manufacturer is 350t/m², the yield strength, f_u , and the modulus of elasticity E of the material used are 28 MPa and 850 MPa respectively.

2.1.3 Properties of the unbound bearing layer

Test procedures for the investigation of mixtures of stone grains, which are intended for unbound bearing layers, are provided by European specifications [10], [11], [12], [13] and [14]. The general characteristics of the gravel material used for the unbound layer are described in more detail elsewhere [12], while a comparison of the densities achieved during compaction are presented in Table 1. The capacity of the unbound base layers was measured through plate-loading tests to determine the values of the deformation for the E_{v1} and E_{v2} modules [TSC 06.200]. The required values of the deformation modules for the unbound bearing layers must meet the requirements in Table 1. It should be noted that the values for the deformation modules are slightly different than expected due to the specimen's preparation particularities. The results for the plate-loading tests measured during the first two cycles for TLS 1 and TLS 3 are presented in Table 2 and Fig. 5.

Table 2. The deformation modules for unbound bearing layers.

D = 155 mm	TLS 1	TLS 3
Determination of E_{v1} module		
u_1 (mm)	1.350	1.264
u_2 (mm)	1.481	1.372
σ_1 (MN/m ²)	0.257	0.257
σ_2 (MN/m ²)	0.356	0.356
E_{v1} (MN/m ²)	87.853	106.563
Determination of E_{v2} module		
u_1 (mm)	1.626	1.440
u_2 (mm)	1.69	1.529
σ_1 (MN/m ²)	0.254	0.255
σ_2 (MN/m ²)	0.349	0.347
E_{v2} (MN/m ²)	172.559	120.168
E_{v2}/E_{v1}	1.96	1.13
The required values of deformation modules for unbound bearing layers		
E_{v2} (MN/m ²)	≥ 90	≥ 90
E_{v2}/E_{v1}	≤ 2.4	≤ 2.4

It is clear from the results presented in Table 1 and 2 that the unbound bearing layer in the case of specimen TLS 3 exhibits a lower density and stiffness compared to TLS 1. Similarly, the asphalt in the surface layer was slightly less compacted in the case of TLS 3 compared to TLS 1. Thus, the more deformable behaviour of specimen TLS 3 (if the effect of the geocell reinforcement is neglected) would be expected during traffic loading.

2.1.4 Properties of subgrade

The commercially available, closed-cell elastomer material Sylodyn [15] has been used to simulate soft ground.

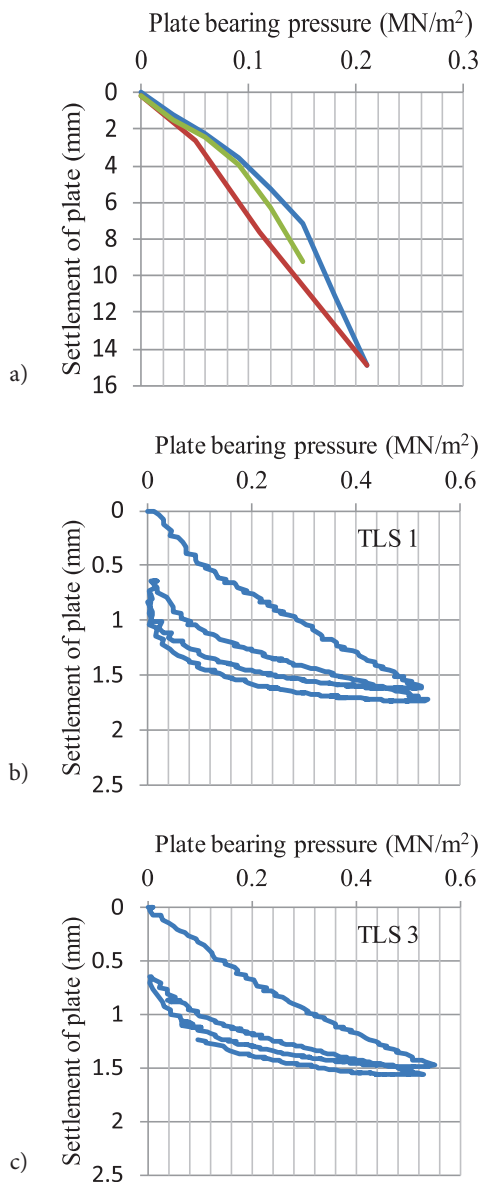


Figure 5. The plate-load test result for the first two cycles for the subgrade layer (a) and the base layer for TLS 1 (b), and TLS 3 (c).

A 5-cm-thick layer of this elastic material enabled equal and constant subgrade conditions for both specimens. Its properties have been tailored in order to meet the requirements for a very low deformation modulus. A typical result of the plate-loading test (loading-blue, unloading-red and reloading-green) of an elastomer material in a subgrade layer is given in Fig. 5a. As can be seen, no permanent deformation developed during cyclic loading of this layer. The Plate Loading Test was carried out in accordance with [16]. It consists of loading a steel plate of known diameter and recording the settlements corresponding to each load increment. The results of the plate-loading test give the modulus of the elastomer material in the subgrade layer equal to 4 MPa. The deformation modulus of the unbound bearing layer of specimens TLS 1 and TLS 3 was measured using the same test method.

2.2 Preparation of the test pavement samples, setup and test procedure

In the first step, a 5-cm-thick elastomer material was positioned to simulate the sub-grade. Next, the unbound granular material was installed and compacted at the moisture content given in Table 1. Approximately 97% (TLS 1) and 95% (TLS 3) of the maximum dry density defined by a modified Proctor compaction test was reached. In the first pavement specimen (TLS 1) only the asphalt layer was installed without any reinforcement. In the second pavement specimen (TLS 3), the geocells were incorporated on the top of the base layer. A very good jointing between the geocells and the asphalt (during the installation phase warm asphalt embraced the top edge of the geocells) was reached. The preparation steps and the installation of the materials for TLS 3 are shown in Fig. 6.

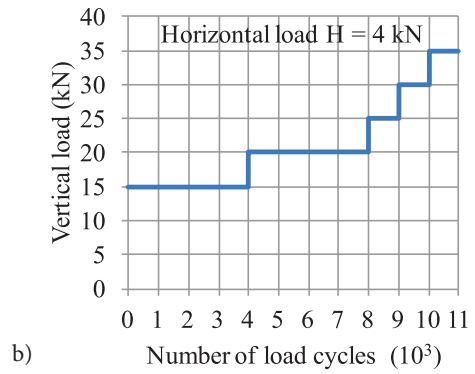
The cyclic loading was then applied through the wheel, through cyclic loading in the vertical and horizontal directions (Fig. 7). Five loading sequences were applied. Vertical loads varied in each loading cycle between the minimum and the maximum value. The minimum value was set to 2 kN for all the loading steps, while the maximum values were 15 kN to 35 kN (see Fig. 7b). The loading process, which includes a load piston and rubber tire, is shown in Fig. 7a. The amplitude of the cyclic horizontal load was approximately one quarter of the vertical amplitude for all the loading steps, while the time diagram of both loads was somehow simultaneous to simulate the rotation of the principal stress. The loading frequency was approximately 0.5 Hz.



Figure 6. Preparation of test pavement specimen.



a)



b)

Figure 7. The loading process for the pavement sections (a) and the loading steps (b).

2.3 TLS test results

Before the application of the cyclic load, a plate-loading test on the asphalt layer for TLS 1 and TLS 3 was performed. The settlements obtained in the second cycle were compared with the settlement obtained using a numerical model. The development of the permanent deformation of the pavement structure without geocells (TLS 1) was measured. Fig. 8a presents the result of the plate-loading test on the asphalt layer for the first two cycles. Fig. 8b shows an increasing amount of permanent deformation at the specimen surface, which arises from the deformations of the whole tested structure after each loading step. Since the test specimens differentiate noticeably only in the presence of the geocells, the observed differences in permanent deformation can be contributed to the effect of the geocells. The development of the permanent deformation of the pavement structure with geocells in the contact between the unbound layer and the asphalt layer (TLS 3) is presented in Fig. 9. The increase in the permanent deformation at the asphalt surface with an increasing number of loading cycles is shown in Fig. 10a for both specimens. For the first 4000 loading cycles, a load of 15 kN was applied. After that, an additional 4000 cycles were applied with a load of 20 kN. For loads of 25 kN, 30 kN and 35 kN, a 1000 load cycles were applied sequentially. The increments of the axial permanent deformation ϵ_1 given as a function of the number of loading cycles N is a good indicator of further long-term deformation. Fig. 10b shows the increments in the vertical permanent deformation ϵ_1 for all the loading steps for the number of loading cycles $N=1000$. The increments arising from Fig. 10a indicate that the installation of the geocells reduced the permanent deformation of the flexural pavement from 12.9 mm (TLS 1) to 6.1 mm (TLS 3), meaning that a decrease in the permanent deformation due to the

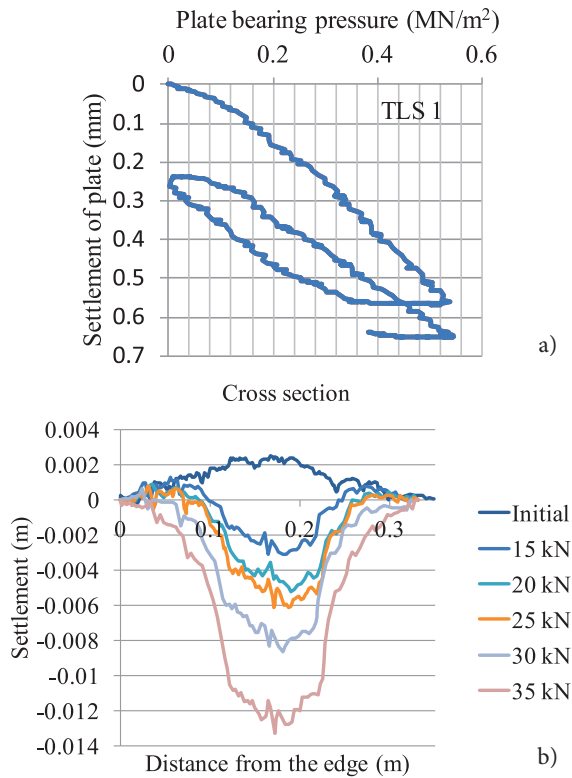


Figure 8. Development of the permanent deformation of the TLS 1: first two cycles of plate-loading test (a), all loading steps (b).

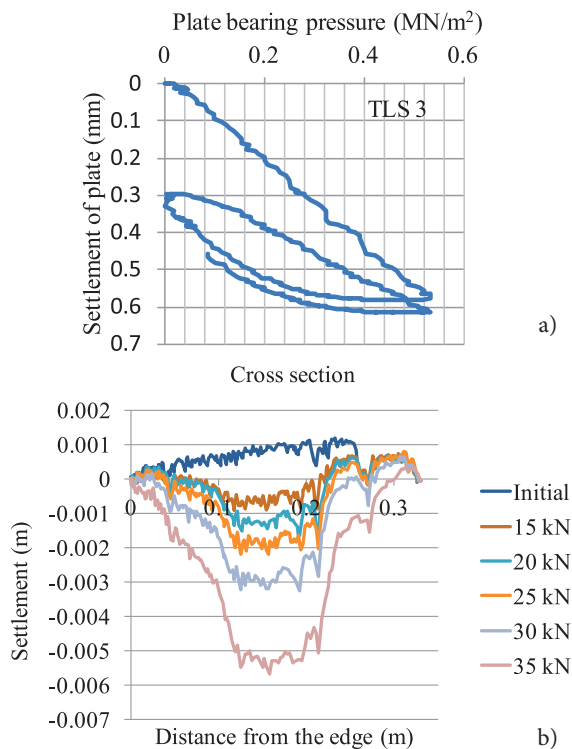


Figure 9. Development of permanent deformation of the TLS 3: first two cycles of plate-loading test (a), all loading steps (b).

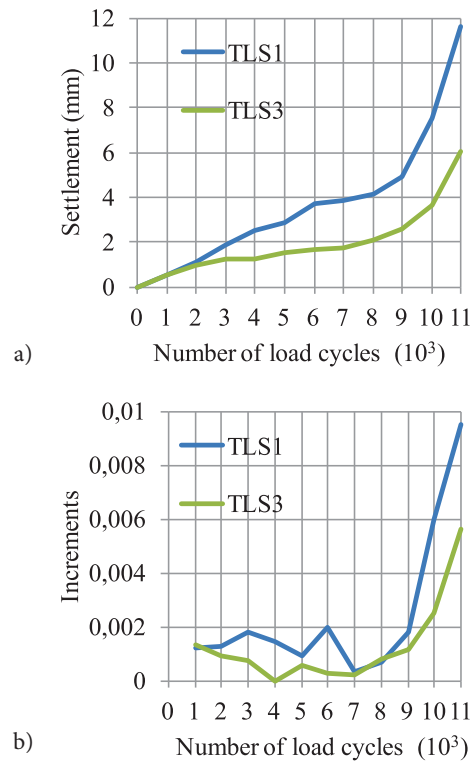


Figure 10. Increase of permanent deformation and the increments of the vertical permanent deformation ϵ_1 for all loading steps, at $N=1000$.

geocell reinforcement is approximately 53%. However, it would be necessary to carry out a sufficient number of loading cycles for an accurate prediction of the development of the permanent deformation.

3 NUMERICAL MODELING

Flexural pavement structures exhibit an elastoplastic behaviour in response to the loading and unloading conditions imposed by traffic loads. Upon unloading, this entails both the recoverable and the permanent deformation components. Therefore, the model for the prediction of the deformation of a geocell-reinforced flexible pavement structure consists of two steps: the resilient and the permanent deformation. The first step is to calculate the elastic stress-strain response for a given wheel load using a finite-element modelling (FEM) program. To estimate the permanent deformation response of the pavement structure the Tseng and Lytton [17] relationship was used (Eq. 14). In this way the lifespan of the pavement structure is evaluated. In this section the numerical models of TLS 1 and TLS 3 are presented.

3.1 The resilient response of the pavement structure

A finite-element analysis program (EverStressFE) was used to simulate the response of flexible pavement systems subjected to a wheel load. The model consists of a three-layer pavement system with finite plan dimensions of 400 mm × 400 mm loaded with a single tire. The material properties, such as the flexural stiffness of the asphalt layer S_a , the flexural stiffness of the geocells S_c , the resilient modulus M_r and the Poisson's ratio μ of the base layer are estimated in this step. The layer thickness and the estimated material properties of these materials are presented in Table 3. The asphalt mixture's stiffness is determined by using the European norm EN 12697-26 [18].

Table 3. Cross-section of pavement structure composition and the mechanical properties of the layers.

Layer	Input data	TLS1	TLS 3
Asphalt layer	Thickness (mm)	30	30
	Flexural stiffness (MPa)	3000	3000
	Poisson's ratio (-)	0.35	0.35
Geocell	Thickness (mm)	/	50
	Flexural stiffness (MPa)	/	2000
	Poisson's ratio (-)	/	0.3
Base layer	Thickness (mm)	430	380
	Resilient modulus (MPa)	173	120
	Poisson's ratio (-)	0.35	0.35
Sub-grade layer	Thickness (mm)	50	50
	Resilient modulus (MPa)	4	4
	Poisson's ratio (-)	0.35	0.35

The resilient modulus of the base layer is estimated by using a repeated load triaxial compression test, according to European norm SIST EN 13286-7:2004 EN 13286-7 [19]. A cyclic load triaxial test was used to determine the resilient strain. The resilient strain ϵ_r is taken as the unloading strain from the maximum dynamic stress down to the static contact stress. The resilient modulus M_r is defined as the relationship between the cyclic deviatoric stress and the resilient axial strain. Several models could be used to describe the resilient behaviour of the unbound granular material in cyclic triaxial tests. The Witczak-Uzan equation [20] is used for the numerical analyses. Uzan [21] proposed a model that considers the effect of the shear stress on the resilient modulus as follows:

$$M_r = K_1 \cdot \theta^{K_2} \cdot \sigma_d^{K_3} \quad (1)$$

where K_1 , K_2 , and K_3 are regression analysis constants evaluated by a multiple regression analyses of the experimental data. Uzan's model considers both the effect of

the bulk stress (θ) and the deviator stress (σ_d), which are directly related to the maximum shear stress

$$\tau_{max} = \frac{\sigma_d}{2} \quad (2)$$

Witczak and Uzan [20] modified the model by including the octahedral shear stress in the model instead of the deviator stress.

$$\frac{M_r}{p_a} = K_1 \cdot p_a \cdot \left(\frac{\theta}{p_a}\right)^{K_2} \cdot \left(\frac{\sigma_d}{p_a}\right)^{K_3} \quad (3)$$

$$\tau_{oct} = \frac{\sqrt{2}}{3} \cdot (\sigma_1 - \sigma_3) \quad (4)$$

The mesh in the FEM is locally refined to obtain a given level of solution accuracy. The rectangular tire contact is modelled with a constant applied stress equal to the tire pressure. The tire pressure is linearly increased with the load. The load per tire F (kN) and the tire width w (mm) were determined. When 15 kN was applied, the tire pressure was 750 kPa and when 35 kN was applied, 1750 kPa was assigned. The FEM (Fig. 11) is designed to analyse complex pavement structures for which analytical solutions do not necessarily exist. Two FE models were solved and the results were compared to the experimental values in order to investigate the accuracy of the FE

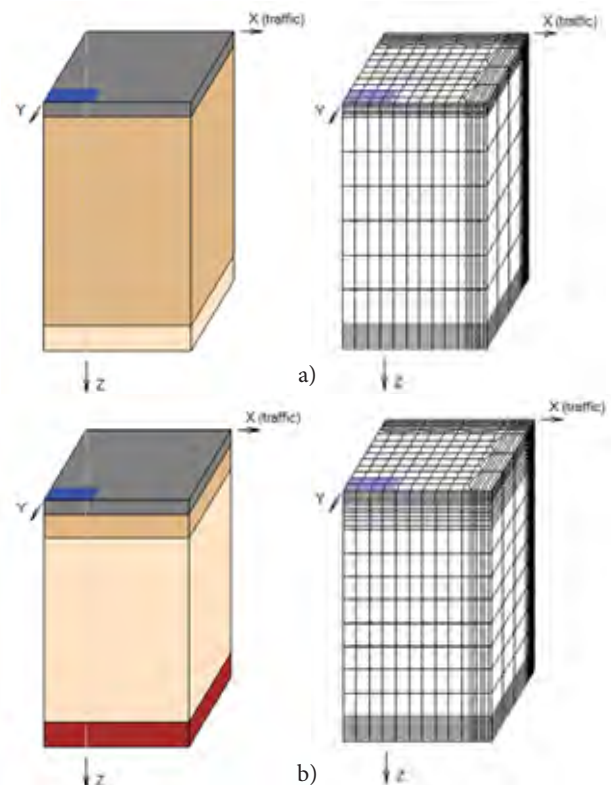


Figure 11. Numerical models of laboratory-tested specimens: without geocell (a) and with geocell reinforcement (b).

Table 4. Calculated horizontal strains at the bottom of the asphalt layer, the average vertical strains and the octahedral shear stress at the base layer.

F (kN)	TLS 1			TLS 3		
	At the bottom of the asphalt layer	Average values in the base layer		At the bottom of the asphalt layer	Average values in the base layer	
	$\epsilon_t (10^{-6})$	τ_{oct} (kPa)	$\epsilon_v (10^{-6})$	$\epsilon_t (10^{-6})$	τ_{oct} (kPa)	$\epsilon_v (10^{-6})$
15	721.2	57.2	1154.5	29.3	21.8	547.2
20	961.6	76.3	1539.3	39.0	29.0	729.7
25	1202.0	95.4	1924.1	48.8	36.3	912.1
30	1442.4	114.4	2308.9	58.5	43.5	1094.5
35	1682.8	133.5	2693.7	68.3	50.8	1276.9

solution. The vertical strain, horizontal strain, and vertical displacement were obtained for both the TLS1 and TLS3 models (see Table 4). The outputs examined were

primarily the maximum vertical (surface) displacement (Fig.12); however, the vertical strains and horizontal strains were also recorded (Fig. 13). The chosen vertical

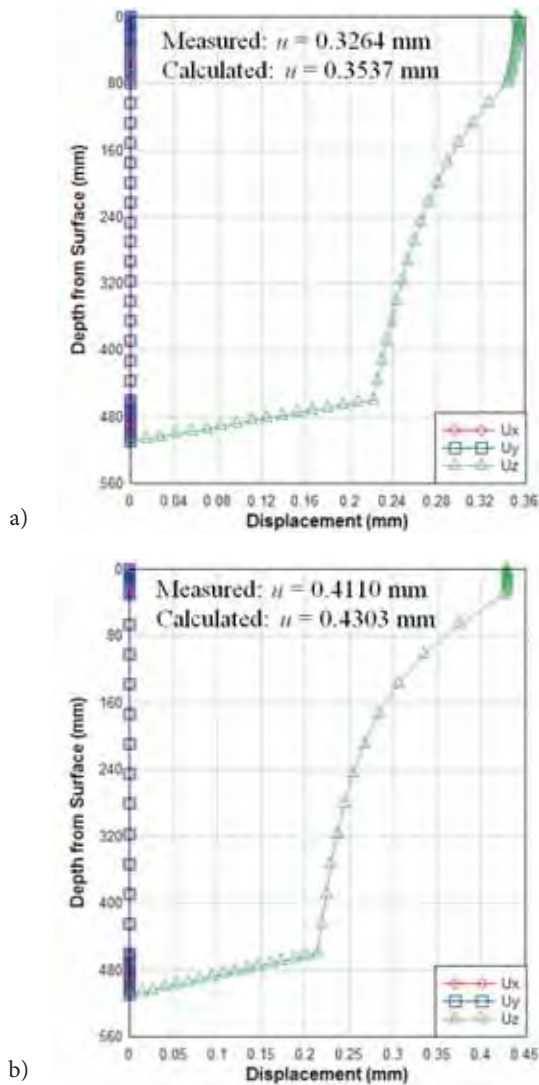


Figure 12. Calculated settlements of the pavement structures using the finite-element modelling.

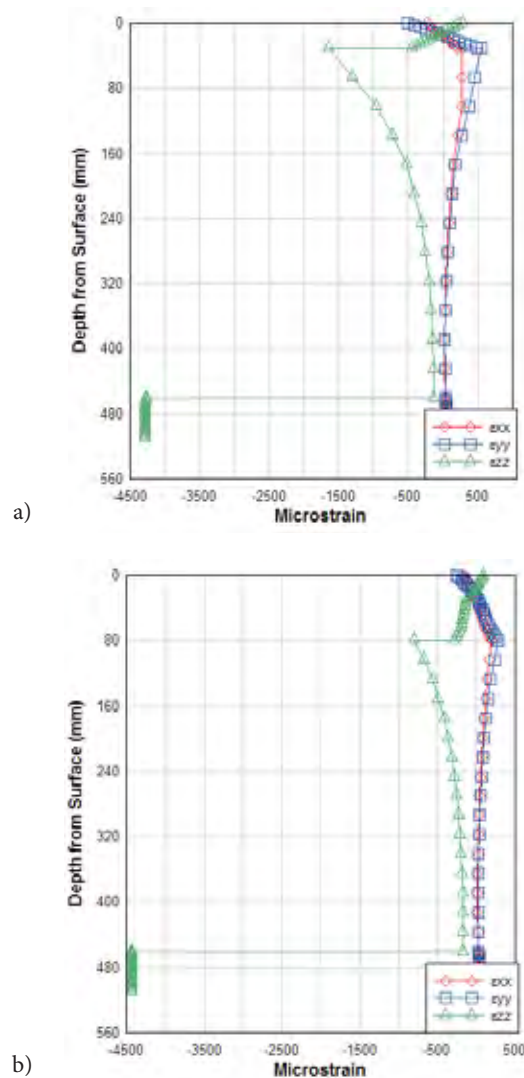


Figure 13. Calculated strains in the cross-section of the test pits: without geocell (a) and with geocell reinforcement (b).

and horizontal strains were the same strains that would be used in the rutting and fatigue prediction models. The settlements in the second cycle of the laboratory test are consistent with the results of the numerical model.

3.2 Permanent deformation of pavement structure

For the prediction of permanent strain in the pavement structure, the following Tseng and Lytton relationship [17] is used:

$$\delta_{1,p}(N) = \frac{\varepsilon_0}{\varepsilon_r} \cdot e^{-\left(\frac{\rho}{N}\right)^\beta} \cdot \varepsilon_v \cdot h \quad (5)$$

where ε_r is the resilient strain and ε_0 is the maximum permanent strain at a very high number of loading cycles, both measured in the laboratory, h is the depth of the layer and ε_v is elastic strain in the pavement layer, computed from the FEM analysis. The parameters ε_0 , ρ and β are defined by laboratory tests using the repeated load triaxial apparatus with the Tseng and Lytton procedure [17].

The determination of the permanent deformations and the failure criteria for gravel materials are based on repeated load tests as defined in EN 13286-7 [14] and SIST EN 13286-7:2004 [19]. The magnitude and development of permanent deformations depends on the static stress state of the material, the magnitude of the repeated load, the magnitude of the spherical and distortional repeated load components and the relationship between them, the number of loading cycles, and the physical properties of the material (density, water content, etc.).

Many researchers, like Paute et al. [22], have tried to relate the permanent deformation after a given number of cycles to the applied stresses (generally the maximum stresses). Some of these relationships also try to couple the effects of both stresses and the number of load cycles. Consider the model of Hornyk et al. [23] and Paute et al. [22], the relation between the axial permanent deformations $\varepsilon_1^p(N)$ and the number of loading cycles N is given by:

$$\varepsilon_1^{p^*} = \varepsilon_1^p(N) - \varepsilon_1^p(100) = A \cdot \left[1 - \left(\frac{N}{100} \right)^{-B} \right] \quad (6)$$

where $\varepsilon_1^p(100)$ is the axial permanent deformation after 100 cycles and $\varepsilon_1^{p^*}(N)$ is the normalized axial permanent deformation at $N > 100$.

Eq. 6 describes the normalized axial permanent deformation, where the parameters A and B define the

deformation growth with the number of loading cycles. Parameter A denotes the limit of the function of the permanent axial deformations, where the parameter B denotes its deflection.

The increments of the axial permanent deformation ε_1 are used as an indicator of further long-term deformation and to determine the slope of the failure line. The increments of the axial permanent deformation are given as a function of the number of loading cycles N in the following form [24]:

$$\frac{d\varepsilon_1^p}{dN} = \frac{A \cdot B}{N} \cdot \left(\frac{N}{100} \right)^{-B} \quad (7)$$

The magnitudes of the parameters A and B depend on the stress level that is expressed by the spherical and deviator stress components

$$p = \sigma_0 + \frac{\sigma_1 + 2 \cdot \sigma_3}{3} \quad (8)$$

$$\sigma_d = \sigma_1 - \sigma_3 \quad (9)$$

The maximum axial permanent deformation or parameter A varies in proportion to the maximum deviator and spherical stresses given in Eq. 8.

$$A = \frac{\frac{\sigma_{d,\max}}{(p_{\max} + p^*)}}{a - b \cdot \frac{\sigma_{d,\max}}{(p_{\max} + p^*)}} \quad (10)$$

where the stress parameter p^* is defined using a section of the failure line with σ_d axis in p - σ_d space. It is determined from a linear equation of test data, according to the method of least-square deviation.

$$\sigma_d = k \cdot p - p^* \quad (11)$$

where k is the slope of the line. The parameters a and b are determined from the test data, with a linear equation of the inverse value of parameter A , using the method of least-square deviation.

$$A^{-1} = a \cdot \left[\frac{\sigma_{d,\max}}{(p_{\max} + p^*)} \right]^{-1} - b \quad (12)$$

The relationship between the parameters a and b gives the slope of the failure line, given by the parameters M and S .

$$\sigma_{d,f} = \frac{a}{b} \cdot (p + p^*) = M \cdot p + S \quad (13)$$

where S is the failure deviatoric stress component σ_d for the spherical stress component $p = 0$ and M is the slope of the failure line. To predict the permanent strain parameter the Tseng and Lytton [17] relationship was used:

$$\varepsilon_{1,p}(N) = \varepsilon_0 \cdot e^{-\left(\frac{\rho}{N}\right)^\beta} \quad (14)$$

where ε_0 is the maximum permanent strain at a very high number of loading cycles, N is the number of cycles and ρ, β are parameters. These parameters are expressed as functions of the octahedral deviator stress τ_{oct} based on a set of repeated load triaxial compression tests. Table 5 shows the parameters which are used for the permanent strain prediction.

The prediction of permanent strain in the pavement structure is calculated using the Tseng and Lytton [17] procedure (Eq. 5). Using the parameters from Table 5, the prediction of long-term deformation for all the loading steps with and without the geocell reinforcements was calculated. Fig. 14 shows the long-term prediction for all the loading steps for the pavement model without geocells (TLS 1) and the comparison of the permanent deformation of TLS 1 and TLS 3 for a loading step of 15 kN. Additionally, the development of permanent deformation is compared with the laboratory test, for all the loading steps conducted with a traffic-load simulator (see Fig. 15).

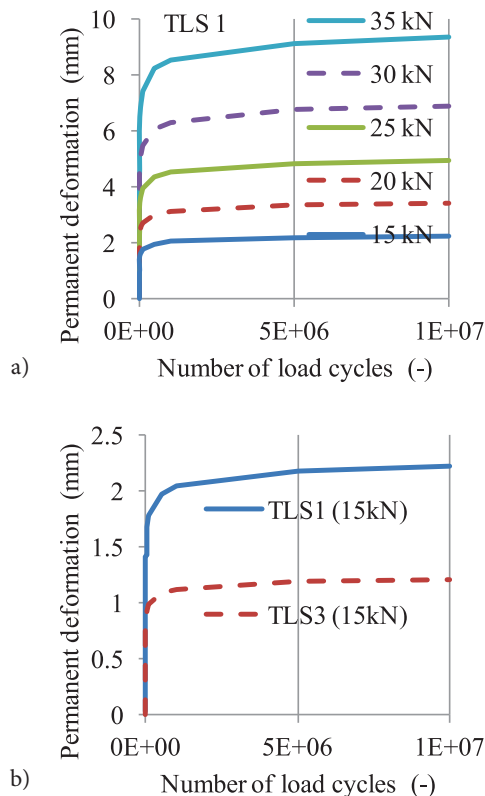


Figure 14. Predicted permanent deformation for TLS 1 and TLS 3 for a large number of cycles.

Table 5. Base-layer permanent strain parameters for TLS 1 and TLS 3.

Permanent strain parameters for TLS 1						
Load (kN)	τ_{oct} (kPa)	ε_v	ε_0	ε_r	ρ	β
15	57.2	0.001155	0.002673	0.000520	0.2135	832
20	76.3	0.001539	0.003492	0.000579	0.2016	808
25	95.4	0.001924	0.004560	0.000646	0.1928	791
30	114.4	0.002309	0.005956	0.000720	0.1860	776
35	133.5	0.002694	0.007779	0.000803	0.1803	764
Permanent strain parameters for TLS 3						
15	21.8	0.000547	0.002712	0.000425	0.2587	916
20	29.0	0.000730	0.002402	0.000442	0.2443	890
25	36.3	0.000912	0.002658	0.000461	0.2337	871
30	43.5	0.001095	0.002943	0.000481	0.2254	855
35	50.8	0.001277	0.003257	0.000501	0.2186	842

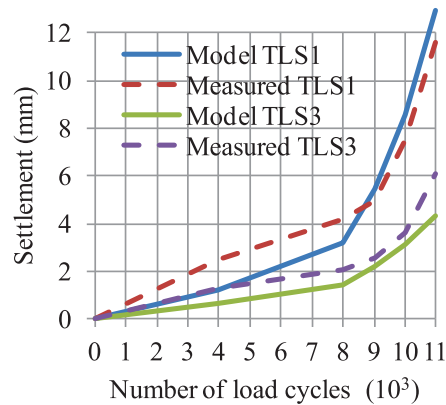


Figure 15. Measured and predicted permanent deformation for TLS 1 and TLS 3 for all the loading steps.

6. CONCLUSION

A pavement structure was constructed in a laboratory to measure the permanent deformation caused by cyclic loading. To reduce the settlement and permanent deformation, geocells were incorporated into the base layer. A laboratory test shows that the permanent deformation was reduced by approximately 53% due to the geocell reinforcement. The laboratory test was also conducted to validate the numerical model for geocells' reinforcement use in pavement design. The numerical model allows the horizontal strain at the bottom of the asphalt layer to be calculated, which is used to determine the fatigue life of the asphalt layer. The results of the numerical model

show that the horizontal strain in the asphalt layer decreases significantly when geocells are used in the pavement structure. Consequently, the fatigue life of the asphalt layer is extended.

REFERENCES

- [1] Kief, O., Rajagopal, K. 2008. Three dimensional cellular confinement system contribution to structural pavement reinforcement. Geosynthetic India '08 Seminar, Hyderabad, India.
- [2] Rea, M., Mitchel, J. 1978. Sand reinforcement using paper grid cells. Proceedings of the regular Meeting , Rocky Mountain Coal Mining Institute, 644-663.
- [3] Dash, S.K., Sireesh, S., Sitharam, T.G. 2003. Model studies on circular footing supported on geocell reinforced sand underlain by soft clay. *Geotextiles and Geomembranes* 21, 197-219. doi:10.1016/S0266-1144(03)00017-7
- [4] Pokharel, S., Han, J., Leshchinsky, D., Parsons, R., Halahmi, I. 2010. Investigation of factors influencing behavior of single geocell-reinforced bases under static loading. *Geotextiles and Geomembranes* 28, 570-578. doi:10.1016/j.geotexmem.2010.06.002
- [5] Yang, X., Han, J., Pokharel, S., Manandhar, C., Parsons, R., Leshchinsky, D., Halahmi, I. 2011. Accelerated pavement testing of unpaved roads with geocellreinforced sand bases. *Geotextiles and Geomembranes* 32, 95-103. doi: 10.1016/j.geotexmem.2011.10.004
- [6] Babu, G., Kumar, P. 2012. An approach for evaluation of use of geocells in flexible pavements. Delhi, India.
- [7] Mengelt, M., Edil, T., Benson, C. 2006. Resilient modulus and plastic deformation of soil confined in a geocell. *Geosynthetics International* 13 (5), 195-205. doi: 10.1680/gein.2006.13.5.195
- [8] Singh, Y., Shankar, R., Jayan, A. 2015. Design of Geocell Reinforced Flexible Pavement. *International Journal of Engineering Research & Technology* 4,3. doi: http://dx.doi.org/10.17577/IJERTV4IS031111
- [9] Geoplast, 2016. The right protection for turf driveway. Available: www.geoplast.it/en/products/green/salvaverde.
- [10] European Standard EN 1097:2003 Tests for mechanical and physical properties of aggregates.
- [11] European Standard EN 1744:2003 Tests for mechanical and physical properties of aggregates.
- [12] European Standard EN 932:2003 Tests for general properties of aggregates.
- [13] European Standard EN 993:2003 Tests for geometrical properties of aggregates.
- [14] European Standard EN13286:2003 Unbound and hydraulically bound mixtures, Tests methods.
- [15] Getzner, 1990. The material for the most stringent requirements, 2016. Available: www.getzner.com/en/products/sylodyn.
- [16] British Standard BS 1377 Part 9:1990.
- [17] Tseng, K., Lytton, R. 1989. Prediction of Permanent Deformation in Flexible Pavements Materials in Implication of Aggregates in the Design, Construction and Performance of Flexible Pavements. Philadelphia: H.G. Schreuders and C.R. Marek.
- [18] European Standard EN 12697-26:2012-03 Bituminous mixtures, The methods for hot mix asphalt; part 26: Stiffness.
- [19] European Standard, SIST EN 13286-7:2004 Unbound and hydraulically bound mixtures - Part 7. Repeated load triaxial test for unbound mixtures.
- [20] Witczak, M., Uzan, J. 1988. The Universal Airport Pavement Design System: Granular Material Characterization. University of Maryland, Department of Civil Engineering, Maryland.
- [21] Uzan, J. 1985. Characterization of Granular Material, Washington D.C.
- [22] Paute, J., Jouvre, P., Martinez, J., Ragenau, E. 1988. Modele de calcul pour le dimensionnement des chaussées souples. *Bulletin de laisons des Laboratoires des Ponts et Chaussées* 156, 21-36.
- [23] Hornyk, P., Corte, J., Paute, J. 1993. Etude des déformations permanentes sous chargements repetes de trois graves non traitees. *Bulletin de laisons des Laboratoires des Ponts et Chaussées* 184, 45-55.
- [24] Ficko, G., Žlender, B. 2005. The analysis of permanent deformations of repeatedly loaded gravels from the Mura region. *Acta Geotechnica Slovenica* 2, 2, 25-37.
- [25] Wasseloo, J., Visser, A., Rust, E. 2009. The stress-strain behaviour of multiple cell geocell packs. *Geotextiles and Geomembranes* 27, 31-38.